Structural and mechanical modifications of GaN thin films by swift heavy ion irradiation

Sophie Eve, Alexis Ribet, Jean-Gabriel Mattei, Clara Grygiel, Eric Hug, Isabelle Monnet

Version of Record: https://www.sciencedirect.com/science/article/pii/S0042207X2100587X
Manuscript_f04014f5451284b31801bfee395f5e43

STRUCTURAL AND MECHANICAL MODIFICATIONS OF GaN THIN FILMS BY SWIFT HEAVY ION IRRADIATION

Sophie EVE[1*], Alexis RIBET[2], Jean-Gabriel MATTEI[2], Clara GRYGIEL[2], Eric HUG[3] and Isabelle MONNET[2]

1 : Laboratoire de Cristallographie et Sciences des Matériaux, ENSICAEN, UMR CNRS 6508, 6 Bd Maréchal Juin 14050 Caen, France ; Sophie.Eve@ensicaen.fr

2 : CIMAP, Normandie Université-CEA-CNRS-ENSICAEN, UMR CNRS 6252, 6 Bd Maréchal Juin 14050 Caen, France

3 : Laboratoire de Cristallographie et Sciences des Matériaux, UNICAEN, UMR CNRS 6508, 6 Bd Maréchal Juin 14050 Caen, France

Abstract

The structural modifications and the evolution of mechanical behavior of gallium nitride (GaN) thin films irradiated by 92 MeV $^{129}Xe^{23+}$ at different fluences have been investigated. The modifications induced by irradiation in GaN have been studied using a combination of high resolution X-ray diffraction and Transmission Electron Microscopy observations coupled to nanoindentation. The crystalline lattice of the GaN is modified by irradiation, with an extension of the lattice along the *c*-direction parallel to the ion path, leading to the development of residual stresses. Correlated to the crystallographic disorder, modification of the deformation mechanisms of the material is observed: damaged areas (highly disordered zones near the surface and black dots deeper in the bulk) hinder the dislocation motion, such as after irradiation, dislocation slip occurs only along the basal plane, and no more prismatic or pyramidal slip is observed. This results in increasing the dislocation loop density, with a subsequent increase in hardness of the GaN film. At higher fluence, the overlapping of the

latent tracks created by swift heavy ions results in a significant decrease in the mechanical characteristics of the thin film, and an amorphous-like material behavior.

Keywords

GaN, irradiation, swift heavy ions, lattice disorder, residual stresses, TEM observations, mechanical behavior

1. Introduction

Because its attractive merits such as high break down voltage, high carrier saturation mobility, wide direct band gap, strong interatomic bonds, and high thermal conductivity, gallium nitride GaN is one of the most promising materials for light emission or detection. Thereby, GaN is currently widely used for the fabrication of opto-electronical components such as Light Emitting Diodes (LEDs), laser diodes, UV sensors or power devices [1, 2]. Moreover, GaN is considered for applications in severe radiative environments, as in spatial or nuclear industry, where the components might be exposed to high energy ionic radiations [3, 4], with energies up to the MeV.

The exposure of semi-conductive materials to ion radiations could result in important modifications of their electrical, optical and mechanical properties, so that the behavior of these compounds under irradiation, within a wide range of energy and projectile mass, is a real issue [5-8]. Indeed, in the case of irradiation in the low energy ion range, the ions lose their energy by elastic collisions with the target nucleus (nuclear energy loss), where atoms could be directly displaced from their lattice sites. In the case of irradiation in the high energy range, the main process of energy deposition is by inelastic interactions with the target electrons (through electronic energy loss), where the projectiles transfer their energy to the electrons of the target. This leads to excitation and ionization processes, and relaxation mechanisms of the lattice through electron-phonon interactions inducing the formation of latent track around the ion path.

With Swift Heavy ions (SHI), the energy deposition is dominated by electronic stopping power. In many materials, predominantly in insulators but also in a few selected semiconductors and metals, continuous or discontinuous tracks could be observed along the ion paths, creating columnar structural modifications. The formation of these latent tracks is only observed above a threshold in electronic stopping power. These tracks could consist of amorphous cylinders embedded in the crystalline matrix. There also exist many other ion-induced structural modifications including amorphous tracks in an amorphous matrix [9-10], tracks consisting of a different crystalline phase than the initial non-irradiated crystal [11-12], and tracks of a more complex core–shell structure as discussed below. The formation of these tracks is by now often explained in literature by a thermal effect, called thermal spike [13], for which the description in complex oxides ceramics is among the more advanced [14].

Majority of researches on GaN thin films have been focused on its optoelectronics characteristics, but an increasing interest developed in the last decades to study its mechanical properties. It has been shown that the lattice mismatch-induced stress between GaN thin films and the available substrates, significantly affecting the threshold power density in simulated emission of GaN optoelectronic devices [15-18]. Suresh *et al.* [19] show that the irradiation of the GaN with energetic particles can produce N vacancy and Ga interstitials, and can result in changes in electrical properties like resistivity, mobility and density of carriers. Furthermore, the irradiation can induce migration of the atoms, leading to internal strain / stress levels into the material [20–24]. Previous observations by Transmission Electron Microscopy (TEM) of SHI irradiated GaN films have shown the development of damage [25-26]. This damage mainly consists in discontinuous latent tracks of a few nanometers in diameter, and appear in GaN along the ions path, for an electronic stopping power threshold of 17 keV/nm. The occurrence of such tracks in GaN after irradiation has been already related by several authors [26-32]. However, regarding GaN, authors agree on the fact that the damage does not lead to a complete amorphisation of the track: whatever the fluence, the material presents a high disorder of its lattice, but remains crystallized [32-36]. An increase in the fluence of the ions results in a recrystallization of overlapping tracks [32] and an increase of the defects concentration and of the size of the damaged zone, from the film surface through its thickness, with a saturation at high fluence

(dechanneling of 80% observed in Rutherford Backscattering Spectroscopy in a channeling direction, RBS-c [34]). At high fluence, a highly disorder zone (HDZ) appears at the near surface [25, 35].

The practical use of GaN in radiative environments requires knowledge of its damage behavior and the effect on its resistance, because, during use, the material may be subjected to mechanical loads arising from for example shock loading in mobile systems. Actually, insuring the long-term stability of the irradiated GaN requires identifying the defects created by irradiation and their effects on the material properties. In this study, we have investigated and correlated the structural and mechanical evolution of GaN thin films irradiated using SHI. Irradiation leads to a distortion of the GaN crystalline lattice, characterized by XRD, and the development of residual stresses in the film. Nanoindentation has been used to investigate the mechanical properties of pristine and irradiated GaN thin films. TEM observations underneath the indents underline an evolution in the deformation mechanisms, linked to the crystalline disorder and damage development caused by SHI.

2. Material and methods

Samples consist in monocrystalline thin films of [0001] epitaxial GaN of 3.5 µm thick, deposited on a [0001] sapphire substrate by MOCVD (Metal Organic Chemical Vapor Deposition). Using this deposition technique, the reactive species are transported in a gaseous form to the substrate and simultaneously pyrolysed, so that growing temperatures range between 900° and 1200° C, after the deposition of a low temperature GaN buffer layer. GaN films were then doped by Si (n-type), at a carrier concentration of about 2.10^{18} /cm^3. The initial dislocations density, correlated to the difference in the lattice parameter between the sapphire substrate and GaN, was about 10^9 /cm^2. These samples were then irradiated at GANIL accelerator (Caen, France), on the IRRSUD line, with 92 MeV $^{129}Xe^{23+}$ ions. Ion irradiation is carried out under normal incidence, at room temperature, and with a flux lower than 5.10^9 ions/cm^2.s, to avoid macroscopic sample heating. The electronic stopping power of the ions decreases along the ion path until the projected range, which is localized in the current setup deep, into the substrate. In order to study the influence of the ion fluence on the modifications induced to the

material, and to identify the damage mechanisms, two fluences were considered: 2.10^{13} and 2.10^{14} ions/cm². Non-irradiated GaN samples were also characterized as reference material.

Using SRIM code [37], the ion energy losses are calculated for 92 MeV $^{129}Xe^{23+}$ in GaN with a material density of 6.15 g.cm^{-3} and displacement energies of 25 eV and 28 eV for Ga and N atoms respectively. At this energy, the electronic regime is predominant on the ion beam path in the nitride. At the surface, the value of the electronic stopping power S_e is 23 keV/nm, above the electronic stopping power threshold $S_{e,th}$ for track formation ($S_{e,th} \approx 17$ keV/nm), corresponding to a depth of about 2 µm [38]. The values of S_n remain very small on the path compared to S_e values: the ENSP ratio (Electronic over Nuclear Stopping Power S_e/S_n) has been determined around 111 at the entrance of the ions in the material, while is about 30 at the end of the GaN layer (after a path of 3.5 µm). Moreover, the mean value of the number of displacements per atom (dpa) created by ballistic collisions over the 3.5 µm of the GaN film has been estimated to 0.05 for a fluence of 2.10^{14} ions/cm². Such values evidence the importance of the S_e compared to the S_n all along the ion path in the GaN thin film.

In order to characterize the modifications of the structure of GaN thin films due to the irradiation by SHI, we made use of the same methodology previously developed to define the damage profiles of Al_2O_3 after irradiation by SHI [39]. Namely, high resolution XRD analyses were performed using with a four-circle Bruker D8 Discover diffractometer using CuK_α radiation (λ = 1.5406 Å). A Göbel mirror was used to obtain a parallel beam. Table 1 presents the different characteristics of each studied reflection. 2θ corresponds to the diffraction angle between the incident beam and the detector, ω the incident angle between the X-ray source and the sample surface. $2\theta = \omega$ setting is used for symmetric geometry whereas $2\theta \neq \omega$ is used for asymmetric geometry. Moreover, χ is the inclination angle (0–90°) between the crystallographic plane and the sample surface, and the probed depth is calculated from the material density, the wavelength of the anode, and a value equal to 90% of I/I_0 intensity ratio. Several reflections were recorded with different optics and geometries allowing observing the whole damaged area, from the surface down to the end of the GaN layer and even more in the substrate. Triple-axis geometry, using a 2-bounce Ge-220 monochromator, an analyzer crystal

and a scintillation detector, enables to obtain high resolution symmetric patterns (0004 reflection), symmetric skew patterns ($10\bar{1}1$, $11\bar{2}2$ and $21\bar{3}3$ reflections, $\chi \neq 0$ and $\chi < 90°$), asymmetric patterns ($10\bar{1}4$ (-) and $11\bar{2}4$ (-) reflections with (-) meaning "grazing" incident beam, $\chi = 0°$) and 2D maps. 2D maps were obtained by taking a series of 2θ-ω patterns (± 0.5° around the reference position) at successive ω values (± 0.5° around the reference position). To probe sample near surface, where the S_e value is the highest, in-plane geometry ($\chi = 90°$) was used. By means of equatorial slits (0.1°) and a LYNXEYE detector in 0D, ($10\bar{1}0$) reflection was recorded with an incident grazing angle of 0.35°, probing sample up to 430 nm. Several software were used to analyze the XRD measurements: Bruker Eva was used of the analysis of the raw patterns, Bruker Leptos for the simulation of the raw 2θ-ω patterns or 2D map representations in direct space, and DxTools [40] for 2D map representations in reciprocal space.

Reflections	2θ (°)	χ (°)	Probed depth (µm)
0004	72.91	0	21.10
$10\bar{1}1$	36.84	61.9	11.20
$11\bar{2}2$	69.10	58.2	20.10
$21\bar{3}3$	119.09	58.8	30.50
$10\bar{1}4$ (-)	82.05	0	15.10
$11\bar{2}4$ (-)	99.95	0	11.20
$10\bar{1}0$	32.39	90	0.43 for $\alpha = 0.35°$

Table 1: Characteristics of measured reflections: Bragg angle 2θ, inclination angle χ and the corresponding probed depth.

The damage created in the GaN films by irradiation ions has been investigated by TEM. For that purpose, samples were prepared using Focused Ion Beam (FIB) station with Ga ions at 30 keV. The voltage is decreased in several steps down to 2 keV for final step in order to avoid damage due to FIB.

TEM lamellas were then examined in a JEOL 2010 FEG TEM operating at 200kV with a point-to-point resolution of 0.23 nm and a lattice resolution of 0.10 nm.

The mechanical behavior of pristine and irradiated GaN thin films has been studied using nanoindentation. This technique is indicated since the tested material volume is scalable with respect to the modified layer thickness, allowing to extract the mechanical characteristics of the film (hardness and elastic modulus), as well as investigating the deformation mechanisms. Tests were conducted using a MTS NanoXP system (MTS Systems Corporation, USA), with a contact module loading head equipped with a three-sided pyramidal Berkovich diamond indenter with a nominal tip radius of curvature of 20 nm. Tests were performed in displacement control by employing the continuous stiffness measurement (CSM) technique, which allows the continuous evaluation of the hardness and the elastic modulus during the indentation loading period. A penetration depth of 200 nm was used, to indent the GaN film at less than 10% of its thickness, and avoid the influence of the sapphire substrate on the measurements. At least 9 indentations were performed for each test, at room temperature. The loading curves were analyzed and the indentation hardness and the elastic modulus were extracted from indentation data, according to the classical Oliver and Pharr method [41].

3. Results and discussion

3.1. Evolution of the GaN lattice parameters induced by irradiation

Fig.1 shows 2D maps in the direct space, recorded for four reflections at different ion fluences up to 2×10^{14} ions/cm². Such maps allow getting a general view of structural modifications induced in irradiated GaN. The dotted lines on the maps help to observe the contribution of the non-irradiated layer of the samples, called reference peaks. On virgin sample and for all reflections, well-defined and intense reflections are observed, assessing for the high crystalline quality of the virgin GaN film. Streaks formation is also noticed, and is explained by the used optics (monochromator and analyzer).

With the increase of the fluence, a large broadening of the (0004) reflection is observed on 2θ axis, meaning that strain is induced by irradiation. Regarding the three other reflections, weaker variations are observed, with a broadening on 2θ axis, correlated to a slight decrease in intensity.

Along ω axis, few modifications with ω angle are depicted for all reflections, as function of the fluence, meaning that very few mosaicity, *i.e.* spread of crystal plane orientations, is present in the material under irradiation. Moreover slight diffuse signal or scattering appears at higher angles for the highest fluence of 2×10^{14} ions/cm², which indicates disorder and compressive area formation.

Fig.2 shows high-resolution pattern of the (0004) reflection for several fluences. Those plots evidence a high intensity reference peak (around 72.9°), corresponding to the reflection of unstrained (reference) zones in the sample. Moreover, with increasing the fluence, different new contributions of relatively high intensity are occurring at lower 2θ angles, linked to the deformation of GaN due to irradiation. Such behavior was already reported by several authors for the (0002) and (0004) reflections with a low resolution [7, 25, 42-44]. The position of these different diffraction peaks allows calculating the deformation of the crystalline lattice, according to the relation:

$$\varepsilon_c = (c_p - c_0)/c_0 \qquad (1)$$

where c_0 and c_p are the value of the c parameter related to the reference peak and the maximum peak (peak occurring with increasing the fluence), respectively. This deformation gradient, appearing for a fluence of 2.10^{13} ions/cm², resulting in a shift of maximum peak corresponding to the maximum tensile strain (at the lowest angle on the pattern) to lower angle or higher strain as the fluence increases. This gap between the reference peak and the peak of maximum strain increases up to a full strain value of about 0.3% +/- 0.05% for 2.10^{14} ions/cm², corresponding to a lattice expansion in the direction of the c-parameter, parallel to the ion beam.

The analysis of the 2θ diffraction patterns associated to the symmetric $(10\bar{1}1)$, $(11\bar{2}2)$ and $(21\bar{3}3)$ reflections, allows to calculate the evolution of the average strain for a- and c-parameters deeper in the film, beyond the extreme surface, using the equations (2) and (1), respectively:

$$\varepsilon_a = (a_i - a_0)/a_0 \qquad (2)$$

The values are given in the Table 2 as a function of the ion fluence, and reveal a slight strain gradient along these directions, higher in *c*-direction than in *a*-direction.

Fluence (ions/cm²)	**ε_a (%)**	**ε_c (%)**
0	0	0
2.10^{13}	- 0.034	0.092
2.10^{14}	- 0.115	0.311

Table 2: Strain of a- and c-parameter of the GaN lattice as a function of 92 MeV $^{129}Xe^{23+}$ fluence, calculated using the four symmetric (0004), (10$\bar{1}$1), (11$\bar{2}$2) and (21$\bar{3}$3) reflections.

Other crystallographic directions have been investigated by recording 2D maps of (10$\bar{1}$4) and (11$\bar{2}$4) asymmetric reflections for different irradiation fluences. As asymmetric geometry associated to a grazing incidence entrance of the X-ray beam is used for these measurements, the material is probed up to 15.1 µm in thickness for the (10$\bar{1}$4) reflection, *i.e.* more than the GaN film thickness. Fig.3 shows 2D maps of the two asymmetric reflections for the virgin sample and the samples irradiated with a fluence of 2×10^{14} ions/cm². Q_z is directly linked to *c*-parameter and Q_x axis to *a*-parameter through the formula for the (10$\bar{1}$4) reflection:

$$Q_z=8\pi/c \quad (3)$$

$$Q_x=4\pi/(a\sqrt{3}) \quad (4)$$

Fine and intense reflection can be observed on the virgin sample with streaks coming from optics. At high fluence 2.10^{14} ions/cm², the occurrence of diffuse zones of smaller intensity around the intense broader reference peak evidences the formation of crystalline disorder, keeping the crystalline coherence of the initial structure.

In order to measure the irradiation effect in the perpendicular direction to the ion beam, the (10$\bar{1}$0) in-plane reflection is also measured as function of the irradiation fluence. This geometry brings also sensitivity to the only topmost irradiated surface layer where only electronic stopping power is

deposited. The evolution of patterns on 2θ axis is not represented as very few modifications of the peak are observed. However, the analysis of these patterns allows to calculate the lattice *a*-parameter extracted from the $(10\bar{1}0)$ position, and the deformation along the *a*-axis. Very slight fluctuation around the virgin value is observed even up to high fluence, and then, we could conclude that no evolution of the in-plane lattice parameter (up to 430 nm) is observed, corresponding to the perpendicular direction to the ion beam.

3.2. Microstructural evolutions of GaN induced by irradiation

Fig.4 presents a TEM micrograph of the sample irradiated with a fluence of 2.10^{14} ion/cm². A Highly Disordered Zone (HDZ) is observed at the extreme surface of the sample, formed by the accumulation of numerous crystallographic defects and resulting in a very different contrast on the TEM image (darker than more in depth in bright field on Fig.4). The thickness of this zone has been evaluated to be of 110 ± 6 nm for this fluence. This zone presents several contrasts of diffraction, meaning that the material remains mainly crystallized, despite the high disorder in its crystalline lattice [32-35]. Beyond this layer, important variations of diffraction contrasts (small areas of black contrasts named black dots) are observed, corresponding to a damaged zone. This contrast decreases as the depth increases, such as almost no black dots are observed near the GaN/sapphire interface. Such an evolution was also observed with 106 MeV ^{238}U (almost the same electronic stopping power than 92 MeV ^{129}Xe) [25].

The damage evolution through the GaN film thickness can be evidenced thanks to the variation of the electron beam intensity detected as a function of the considered depth. The transmitted intensity is related to the diffraction contrasts of the different zones of the sample, linked to the presence of black dots. As presented in the insert in Fig.4, a peak of intensity is detected at the sample surface, corresponding to the platinum layer deposited during the sample preparation. At the end of the depth, a sharp increase in the transmitted intensity is observed, corresponding to the transition from the damaged GaN film to the Al_2O_3 substrate at the interface. Just before this sharp increase, the transmitted intensity is higher than in the zone between the HDZ and this zone. This is due to the fact that at this depth there are much less black dots. Thanks to these observations, the depth of the

damaged zone of the GaN film can be estimated to about 2.8 µm (see insert in Fig.4). We can note the presence of contrast in the sapphire, linked to the presence of disorder since the ion electronic stopping power is above the threshold of damage creation. Just under the interface, there is an amorphous layer of Al_2O_3 (few tens of nanometer) followed by a defected but still crystalline material. This is in agreement with the known evolution of sapphire under SHI [39].

Observations of samples irradiated with lower ion fluences reveal an important damage, with a high density of "black dots", decreasing as a function of the depth, and almost no black dots after 2 µm in depth. The HDZ is hardly visible at this fluence (2.10^{13} ions/cm²), at most few nm.

3.3. Estimation of the stresses induced in the GaN film by irradiation

Residual stresses developed in the material can be computed based on the values of deformation calculated previously from XRD data and the elastic parameters of the GaN. The development of residual stresses in thin films could be linked to either mismatch in lattice parameters between the substrate and the film (growth stress), phase transformations or plastic deformation of the materials, as well as a consequence of materials irradiation. In the last case, the hydrostatic component of the stress is an isotropic tensile stress, related to the swelling of the material due to the formation of point defects, defects accumulation or ions tracks development. The biaxial component is a compressive stress linked to the in-plane influence of the non-irradiated material on the damaged layers. The increasing quantity of defects can thus induce expansion or contraction of the unit cell in the crystal lattice, and three-dimensional stress may appear in samples if the defects are uniformly distributed in the crystal lattice [8, 42].

According to the basic linear and isotropic elastic theory, out-of-plane (along the *c*-direction) and in-plane (along the *a*-direction) strain components for the hexagonal structure of (0001)-GaN layer, ε_a and ε_c, are the superposition of biaxial and hydrostatic strains [43], according to the relations:

$$\varepsilon_c = \varepsilon_c^b + \varepsilon_h \quad (5)$$

and:

$$\varepsilon_a = \varepsilon_a^b + \varepsilon_h \quad (6)$$

with:

$$\varepsilon_h = \frac{1-\nu}{1+\nu}\left(\varepsilon_c + \frac{2\nu}{1-\nu}\varepsilon_a\right) \quad (7)$$

and the Poisson coefficient:

$$\nu = \frac{C_{13}/C_{33}}{1+(C_{13}/C_{33})} \quad (8)$$

where ε_h is the hydrostatic strain, ε_c^b and ε_a^b are the biaxial strains in the *c*- and *a*-directions, respectively, and C_{ij} are the elastic constants of GaN.

Biaxial stress in the basal plane is defined such as the stress component in the crystallographic *b*-direction equals the component in the *a*-direction, whereas the biaxial stress component in the *c*-direction equals zero. For the hydrostatic stress σ_h, the stress in the *a*-, *b*- and *c*-directions are equal. Accordingly, hydrostatic and in-plane biaxial stresses in the GaN layer can then be determined from the relationships:

$$\sigma_h = \frac{E}{1-2\nu}\varepsilon_h \quad (9)$$

and:

$$\sigma_b = M_f\, \varepsilon_a^b \quad (10)$$

with:

$$M_f = C_{11}+C_{12} - 2\, C_{13}^2/C_{33} \quad (11)$$

M_f is the biaxial elastic modulus for a material with a hexagonal structure strained along the [0001] crystallographic direction. Using C_{11} = 390 GPa, C_{12} = 145 GPa, C_{13} = 104.5 GPa, C_{33} = 401.5 GPa, according to [42, 44-48], the value of ν = 0.207 for the Poisson coefficient, and M_f = 480.6 GPa for the biaxial elastic modulus, are obtained from Eq. (8) and (11), respectively.

The hydrostatic stress in the GaN film is then computed from (9), using the value of Poisson coefficient calculated from (8), a value of E = 286.5 GPa for the Young's modulus [42, 47-48], and the value of the hydrostatic strain obtained from (7). The biaxial stress can be calculated from (10), substituting the values of biaxial strain in the *a*-direction and biaxial elastic modulus.
In order to compute the variation of the stresses with the irradiation fluence, the first hypothesis has been taken that the values of the elastic constants C_{ij} and of the Young's modulus E are constant under irradiation, whatever the fluence, what we know to not be correct but it is a start point to approach absolute values.

Fig.5 displays the evolution of the hydrostatic and the biaxial stresses developing in GaN, as a function of the fluence, computed from the XRD high resolution patterns of the (0004), $(10\bar{1}1)$, $(11\bar{2}2)$ and $(21\bar{3}3)$ reflections. Both the hydrostatic and the biaxial stress increase up to a fluence of 2.10^{14} ions/cm², linked to the increasing damage of the GaN film created by irradiation.

The relationship between the biaxial stress in the film and the electronic stopping power S_e of the ions is well established: biaxial stresses increase with the S_e of ions, as already observed by Moisy *et al.* [38], who concluded that when the projectiles exhibit an electronic stopping power S_e lower than the ion track formation threshold $S_{e,th}$ of 17 keV/nm, the measured stress values stay relatively low, whereas the formation of ion tracks implies large biaxial stress in the GaN layer, of about 1.5 GPa here. Such an increase in the residual stresses has been also observed by Zhang *et al.* [44] in a 3 µm-thick GaN film under irradiation by Xe 308 MeV ions.

3.4. Mechanical characterization of the GaN films by nanoindentation

The evolution of the mechanical properties of the material induced by the microstructural modifications, the damage and the development of residual stresses in the GaN film due to irradiation, has been investigated using the nanoindentation technique.

Fig.6 shows the average CSM load-hold-unload curve as a function of depth obtained by nanoindentation of non-irradiated and irradiated GaN, for a maximum indentation depth of 200 nm, i.e. less than 10% of the film thickness, in order to avoid any eventual influence of sapphire substrate on GaN properties. An elasto-plastic behavior of the pristine and irradiated GaN films is observed, correlated to an important residual deformation after unloading, of about 70%. As compared to the pristine GaN, the load requested for the indenter penetration into the material is higher for the sample irradiated with the fluence of 2.10^{13} ions/cm², and decreases for the fluence of 2.10^{14} ions/cm².

Fig.7 presents the evolution of the elastic modulus and the hardness of the materials as a function of the fluence, evaluated using Oliver and Pharr method [41]. It is noticed that the pristine GaN and the sample irradiated at 2.10^{13} ions/cm² exhibit a rather stable value of modulus and hardness along the penetration depth. On the contrary, the sample irradiated with the highest fluence of 2.10^{14} ions/cm² shows a different behavior, with an increase of the mechanical parameters as a function of the penetration, which is closed to the behavior of an amorphous material.

The values of the modulus and the hardness of the pristine GaN film, measured in the stable domain, have been evaluated at 260 ± 6 GPa and 18 ± 1 GPa, respectively. These values are in good agreement with previous studies on epitaxial GaN films characterized by nanoindentation using a Berkovich tip, and slightly larger than parameters obtained by different indentor tips, mainly because of variations in the specific tip-surface contact configuration and stress distribution inherent to each measuring methods [17, 33, 49-50].

Nanoindentation results show that the material irradiated using the fluence of 2.10^{13} ions/cm² exhibits a value of hardness higher than the pristine material, of 24 ± 1 GPa, with a similar modulus. Simulations show that the mean free path of 92 MeV $^{129}Xe^{23+}$ in GaN is around 8 µm in these experimental conditions [9]. That means that the SHI penetrate the total thickness of the GaN film, and implant into the sapphire substrate, so that the drastic change of the mechanical properties of the material cannot be caused by the presence of implanted Xe ions into the material. Then, it is argued

that the microstructural modifications of the GaN induced by the irradiation can explain the evolution of the mechanical behavior of the GaN under irradiation. It has been shown that the penetration of the Xe ions in the material leads to damage in the crystalline lattice, with an increase of the defects concentration from the film surface through its thickness, and that this damage increases with the fluence, up to a maximum when the damage saturation is reached.

As previously discussed, TEM observations of sample irradiated with a fluence of 2.10^{13} ions/cm² presents a high density of "black dots" in the region ear the sample surface, and a very thin HDZ of few nm. The high density of defects resulting from irradiation gives rise to an increase of the stresses in the material, as shown in the previous section. The relaxation of the stresses by plastic deformation induces the nucleation and the set of dislocations motion. An increase in strength of irradiated hexagonal closed packed structure materials has already been reported in the literature [51], and attributed to the presence of a high density of small radiation-induced loops (here, "black dots"), that act as obstacles against dislocation glide. According to the damage observed in GaN sample irradiated with a fluence of 2.10^{13} ions/cm², such a mechanism might take place and results in a subsequent hardening of the material after irradiation.

In order to support this analysis, TEM lamella underneath the indented spot have been cut into pristine and irradiated GaN with a fluence of 2.10^{13} ions/cm². TEM images of these cross sections are presented in Fig.8.

As suggested by Bradly *et al.* [16] and by Jian [18], Fig.8a clearly displays that, within the pristine film, the deformation mechanisms are primarily driven by dislocation slip activity. Several types of gliding planes for dislocations are clearly evidenced. First, there are dislocations gliding in {0001} basal planes, parallel to the interface of GaN film-sapphire substrate. In addition, dislocations gliding in prismatic planes (*i.e.* perpendicular to the basal planes) are also visible. Finally, some dislocations are gliding in pyramidal planes in the plastically deformed area (slip bands oriented at ~60° to GaN surface).

Fig.8b displays a TEM image underneath the indented spot after indentation of GaN thin film irradiated with a fluence of 2.10^{13} ions/cm². It clearly shows a reduction in the number of available slip planes, as only slip bands aligning parallel to the interface of GaN film-sapphire substrate along the

{0001} basal planes could be observed, but no more the slip bands oriented at ~60° to GaN surface previously observed under the indenter print in non-irradiated GaN film, or dislocation gliding in prismatic planes. As a consequence, since the main deformation mechanism in GaN film is dislocation slip mechanism, the irradiated GaN thin films become less susceptible to plastic deformation. This effect is observed in Fig.6, which shows an extent of the elastic recovery of the sample irradiated with a fluence of 2.10^{13} ions/cm², *i.e.* the reduction of the residual deformation observed on the loading curves. Such phenomenon of freezing of slip planes has already been reported in implanted GaN thin films [16, 50]. Both the destruction of long range crystalline order, and the residual stresses within the GaN film, hinders dislocation slip.

Finally, we noticed in Fig.7 that the GaN irradiated with the highest fluence of 2.10^{14} ions/cm² shows a mechanical behavior close to the one of an amorphous material, with an increase of the mechanical parameters as a function of the penetration. Moreover, the values of the modulus and the hardness, measured at a penetration of 200nm, are much smaller than the ones measured for pristine GaN, being estimated to 209 ± 3 GPa and 14.4 ± 0.2 GPa, respectively. The surface of the highly-irradiated GaN layer, presenting an extended HDZ at the extreme surface and an in-deep disorder could induce this smaller value of the modulus. Moreover, the densification resulting from compression and shear strain developed under the indenter tip, leads to easier plastic deformation, thus rendering the irradiated layer softer, exhibiting a smaller hardness value.

4. Conclusion

In this work, GaN/Al_2O_3 samples have been irradiated with 92 MeV $^{129}Xe^{23+}$ at several fluences. Main results obtained in this research can be summarized by the following points:

- According to XRD measurements, irradiation of GaN results in an average structure closed to the initial one with an extension of the lattice along the *c*-direction, parallel to the ions path, and almost no variations along the *a*-direction, perpendicular to ion beam. This deformation of the crystalline lattice causes the development of residual stresses within the GaN film.

- TEM observations have highlighted the existence of a HDZ near the free surface of the film, which grows with increasing the fluence, and the formation of black dots below. These results highlight that higher strain level develops near the surface and decrease as a function of depth.
- Nanoindentation was used to evaluate the impact of the irradiation on the mechanical behavior. The high crystalline disorder caused by irradiation, even larger as the ions fluence increases, and the development of residual stress within the film, significantly hinder the dislocations slip mechanism, reducing the GaN ability to deform plastically, and increasing the surface hardness for the sample irradiated with a fluence of 2.10^{13} ions/cm².
- The overlapping of the latent tracks for the fluence of 2.10^{14} ions/cm² results in a decrease of the strength of GaN, correlated to an amorphous-like mechanical behavior, probably linked to a growth of the ZFE at the extreme surface at high fluence.

Such modifications of the GaN crystallographic structure and mechanical behavior by irradiation with SHI have to be tackled for considering the practical use of GaN thin films based optics in radiative environments.

Acknowledgements

The experiments were performed at the Grand Accélérateur National d'Ions Lourds (GANIL), Caen, France, and the authors thank the CIMAP, the CIRIL and GANIL staff for their helps. This work was partially supported by the ANR funding "Investissements d'avenir" ANR-11-EQPX-0020 and ANR10-LABX-09-01 LabEx EMC3, the FEDER and by the Region Basse-Normandie.

References

[1] H. Morkoc, S.N. Mohammad, High-Luminosity Blue and Blue-Green Gallium Nitride Light-Emitting Diodes, Science 267 (1995) 51-55.

[2] G. Fasol, Room-Temperature Blue Gallium Nitride Laser Diode, Science 272 (1996) 1751-1752.

[3] D.H. Lien, Y.H. Hsiao, S.G. Yang, M.L. Tsai, T.C. Wei, S.C. Lee, J.H. He, Harsh photovoltaics using InGaN/GaN multiple quantum well schemes, Nano Energy 11 (2015) 104-109.

[4] L. Lv, J.G. Ma, Y.R. Cao, J.C. Zhang, W. Zhang, L. Li, S.R. Xu, X.H. Ma, X.T. Ren, Y. Hao, Study of proton irradiation effects on AlGaN/GaN hich electron mobility transitors, Microelectron. Reliab. 51 (2011) 2168-2172.

[5] V. Suresh Kumar, M. Senthil Kumar, P. Puviarasu, J. Kumar, T. Mohanty, D. Kanjilal, K. Asokan, A. Tripathi, M. Fontana, A. Camarani, Investigations on the 100 MeV Au^{7+} ion irradiation of GaN, Semicond. Sci. Technol. 22 (2007) 511-516.

[6] K. Son, A. Liao, G. Lung, M. Gallegos, T. Hatake, R.D. Harris, L.Z. Scheick, W.D. Smythe, GaN-based High Temperature and Radiation-Hard Electronics for Harsh Environments, Nanosci. Nanotechnol. Lett. 2 (2010) 89-95.

[7] J. Gou, L.Q. Zhang, C.H. Zhang, Y. Song, Y.T. Yang, J.J. Li, Y.C. Meng, H.X. Li, Effects of irradiation of 290 MeV U-ions in GaN epi-layers, Nucl. Instrum. Methods Phys. Res. B 307 (2013) 89-92.

[8] P.P. Hu, J. Liu, S.X. Zhang, K. Maaz, J. Zeng, H. Guo, P.F. Zhai, J.L. Duan, Y.M. Sun, M.D. Hou, Raman investigation of lattice defects and stress induced in InP and GaN films by swift heavy ion irradiation, Nucl. Instrum. Methods Phys. Res. B 372 (2016) 29-37.

[9] M. Toulemonde, C. Dufour, E. Paumier, Transient thermal process after a high energy heavy-ion irradiation of amorphous metals and semiconductors, Phys. Rev. B 46 (1992) 14362-14369.

[10] S. Klaumünzer, Ion tracks in quartz and vitreous silica, Nucl. Instrum. Methods B 225 (2004) 136–153.

[11] B. Schuster, F. Fujara, B. Merk, R. Neumann, T. Seidl, C. Trautmann, Response behavior of ZrO2 under swift heavy ion irradiation with and without external pressure, Nucl. Instrum. Methods B 277 (2012) 42–52.

[12] A. Benyagoub, F. Couvreur, S. Bouffard, F. Levesque, C. Dufour, E. Paumier, Phase transformation induced in pure zirconia by high energy heavy ion irradiation, Nucl. Instrum. Methods B 175–177 (2001) 417–421.

[13] F. Seitz, J.S. Koehler, Displacement of atoms during irradiation, Solid Stata Phys. 1 (1956) 305-448.

[14] M. Lang, R. Devanathan, M. Toulemonde, C. Trautmann, Advances in understanding of swift heavy-ion tracks in complex ceramics, Curr. Opin. Solid. State Mater. Sci. 19 (2015) 39-48

[15] J.L. Weyher, M. Albrecht, T. Wosinski, G. Nowak, H.P. Strunk, S. Porowski, Study of individual grown-in and indentation-induced dislocations in GaN by defect-selective etching and transmission electron microscopy, Mater. Sci. Eng. B 80 (2001) 318-321.

[16] J.E. Bradby, S.O. Kucheyev, J.S. Williams, J.W. Leung, M.V. Swain, P. Munroe, G. Li, M.R. Philips, Indentation-induced damage in GaN epilayers, Appl. Phys. Lett. 80 (2002) 383-385.

[17] S.O. Kucheyev, J.E. Bradby, J.S. Williams, C. Jagadish, M. Toth, M.R. Phillips, M.V. Swain, Nanoindentation of epitaxial GaN films, Appl. Phys. Lett. 77 (2000) 3373-3375.

[18] S.R. Jian, Berkovich indentation-induced deformation behaviors of GaN thin films observed using cathodoluminescence and cross-sectional transmission electron microscopy, Appl. Surf. Sci. 254 (2008) 6749-6753.

[19] S. Suresh, V. Ganesh, U.P. Deshpande, T. Shripathi, K. Asokan, D. Kanjilal, K. Baskar, Structural, optical, and electrical characteristics of 70 Mev Si5+ ion irradiation-induced nanoclusters of gallium nitride, J. Mater. Sci. 46 (2011) 1015–1020.

[20] M. Senthil Kumar, G. Sonia, D. Kanjilal, Electrical and optical isolation of GaN by high energy ion irradiation, Nucl. Instr. Meth. Phys. Res. B 207(2003) 308–313.

[21] D.C. Look, D.C. Reynolds, J.W. Hemsky, J.R. Sizelove, R.L. Jones, R.J. Molnar, Defect Donor and Acceptor in GaN, Phys. Rev. Lett. 79 (1997) 2273– 2276.

[22] G. Devaraju, A.P. Pathak, N. Sathish, N. Srinivasa Rao , V. Saikiran , A.I. Titov, Electronic stopping dependence of ion beam induced modifications in GaN, Nucl. Instr. Meth. Phys. Res. B 269 (2011) 890–893.

[23] G. Devraju, S.V.S. Nageswara Rao, N. Srinivasa Rao, V. Saikiran, T.K. Chan, T. Osipowicz, M.B.H. Breese, A.P. Pathak, Ion beam-mixing effects in nearly lattice-matched AlInN/GaN heterostructures by swift heavy ion irradiation, Radiation Effects and Defects in Solids 167 (2012) 506-511.

[24] L.Q. Zhang C.H. Zhang, J.J. Li, Y.C. Meng, Y.T. Yang, Y. Song, Z.N. Ding, T. X. Yan, Damage to epitaxial GaN layer on Al_2O_3 by 290-MeV $^{238}U^{32+}$ ions irradiation, Scientific Report 8 (2018) 4121.

[25] M. Sall, I. Monnet, F. Moisy, C. Grygiel, S. Jublot-Leclerc, S. Della–Negra, M. Toulemonde, E. Balanzat, Track formation in III-N semiconductors irradiated by swift heavy ions and fullerene and re-evaluation of the inelastic thermal spike model, J. Mater. Sci. 50 (2015) 5214-5227.

[26] J-G.Mattei, M.Sall, F.Moisy, A.Ribet, E.Balanzat, C.Grygiel, I.Monnet, Fullerene irradiation leads to track formation enclosing nitrogen bubbles in GaN material, Materialia 15 (2021) 100987.

[27] S. Strite, H. Morkoc, GaN, AlN, and InN: A review, J. Vac. Sci. Technol. B 10 (1992) 1237-1166.

[28] N. Satish, S. Dhamodaran, A.P. Pathak, M. Ghanashyam Krishna, S.A. Khan, D.K. Avasthi, A. Pandey, R. Muralidharan, G. Li, C. Jagadish, HRXRD, AFM and optical study of damage created by swift heavy ion irradiation in GaN epitaxial layers, Nucl. Instr. Meth. Phys. Res. B 256 (2007) 281-287.

[29] M. Karlušić, R. Kozubek, H. Lebius, B. Ban-d'Etat, R.A. Wilhelm, M. Buljan, Z. Siketić, F. Scholz, T. Meisch, M. Jakšić, S. Bernstorff, M. Schleberger, B. Šantić, Response of GaN to energetic ion irradiation: conditions for ion track formation, J. Phys. D: Appl. Phys.48(2015) 325304.

[30] S.J. Pearton, J.C. Zolper, R.J. Shul, F. Ren, GaN: Processing, defects, and devices, J. Appl. Phys. 86 (1999) 1-78.

[31] C.J. Shen, J.M. Greenberg, W.A. Schutte, E.F. van Dishoeck, Cosmic ray induced explosive chemical desorption in dense clouds, Astronomy and Astrophysics 415 (2004) 203-215.

[32] M. C. Sequeira, J.G. Mattei, H. Vazquez, F. Djurabekova, K. Nordlund, I. Monnet, P. Mota-Santiago, P. Kluth, C. Grygiel, S. Zhang, E. Alves and K. Lorenz, Unravelling the secrets of the resistance of GaN to strongly ionising radiation, Comm. Phys. 4 (2021).

[33] S.O. Kucheyev, J.S. Williams, S.J. Pearton, Ion Implantation into GaN, Mater. Sci. Eng. 33 (2001) 51-107.

[34] S.O. Kucheyev, H. Timmers, J. Zou, J.S. Williams, C. Jagadish, G. Li, Lattice damage produced in GaN by swift heavy ions, J. Appl. Phys. 95 (2004) 5360-5365.

[35] F. Gloux, T.Wojtowicz, P. Ruterana, K. Lorenz, E. Alves, Transmission electron microscopy investigation of the structural damage formed in GaN by medium range energy rare earth ion implantation, J. Appl. Phys. 100 (2006) 073520.

[36] V. Baranwal, A.C. Pandey , J.W. Gerlach , B. Rauschenbach , H. Karl , D. Kanjilal , D.K. Avasthi, Rapid thermal and swift heavy ion induced annealing of Co ion implanted GaN films, J. Appl. Phys. 103 (2008) 124904.

[37] J.F. Ziegler, J.P. Biersack, U. Littmark, The Stopping and Range of Ions in Matter - SRIM, Pergamon, New York, 1985.

[38] F. Moisy, M. Sall, C. Grygiel, A. Ribet, E. Balanzat, I. Monnet, Optical bandgap and stress variations induced by the formation of latent tracks in GaN under swift heavy ion irradiation, Nucl. Instr. Meth. Phys. Res. B 431 (2018) 12–18.

[39] A. Ribet, J-G. Mattei, I. Monnet, C. Grygiel, Damage depth profile in α-Al_2O_3 induced by swift heavy ions, Nucl. Instr. Meth. Phys. Res. B 445 (2019) 41–45.

[40] A. Boulle, DXTools: processing large data files recorded with the Bruker D8 diffractometer, J. Appl. Cryst. 50 (2017) 967-974.

[41] W.C. Oliver, G.M. Pharr, An improved technique for determining hardness and elastic-modulus using load and displacement sensing indentation experiments, J. Mater. Res. 7 (1992) 1564-1583.

[42] V.S. Harutyunyan, A.P. Aivazyan, E.R. Weber, Y. Kim, Y. Park, S.G. Subramanya, High resolution x ray diffraction strain stress analysis of GaN_sapphire heterostructures, J. Phys. D Appl. Phys. 34 (2001) 35-39.

[43] C. Kisielowsk, J. Kruger, S. Ruvimov, T. Suski, J.W. Ager III, E. Jones, Z. Liliental-Weber, M. Rubin, E.R. Weber, M.D. Bremser, R.F. Davis, Strain related phenomena in GaN thin films, Phys. Rev. B 54 (1996) 745-753.

[44] L.M. Zhang, H. Zhang, L.Q. Zhang, X.J. Jia, T.D. Ma, Y. Song, Y.T. Yang, B.S. Li, Y.F. Jin, Structural and optical study of irradiation effect in GaN epilayers induced by 308 MeV Xe ions, Nucl. Instrum. Methods Phys. Res. B 269 (2011) 1782–1785.

[45] E. Varadarajan, R. Dhanasekaran, D.K. Avasthi, and J. Kumar, Structural, optical and electrical properties of high energy irradiated Cl-VPE grown gallium nitride, Mater. Sci. Eng. B 129 (2006) 121–125.

[46] V. Suresh Kumar, J. Kumar, P. Puviarasu, S. Munawar Basha, D. Kanjilal, and K. Asokan, Effect of 100mev Ni9+ ion irradiation on MOCVD grown n-GaN, Physica B: Condens. Matter 406 (2011) 4210–4213.

[47] M.A. Moram and M.E. Vickers, X-ray diffraction of III nitrides. Rep. Prog. Phys. 72 (2009) 1-40.

[48] S. Pereira, M.R. Correia, E. Pereira, K.P. ODonnell, E. Alves, A.D. Sequeira, N. Franco, I.M. Watson, C.J. Deatcher, Strain and composition distributions in wurtzite In-GaN/GaN layers extracted from x-ray reciprocal space mapping, Appl. Phys. Lett. 80 (2002) 3913–3915.

[49] C.H. Tsai, S.R. Jian, J.Y. Juang, Berkovich nanoindentation and deformation mechanisms in GaN thin films, Appl. Surf. Sci. 254 (2008) 1997-2002.

[50] P. Kavouras, P. Komninou, T. Karakostas, Effects of ion implantation on the mechanical behavior of GaN films, Thin Solid Films 515 (2007) 3011-3018.

[51] F. Onimus, L. Dupuy, F. Mompiou, In situ TEM observation of interactions between gliding dislocations and prismatic loops in Zr-ion irradiated zirconium alloys, Progress in Nuclear Energy 57 (2012) 77-85.

Fig.1: 2D maps for four reflections of GaN irradiated at different fluences. 2θ axis is from left to right, ω axis from bottom to top, maps correspond to a variation of ± 0.5° around the reference value for 2θ and ω. The same scale is used on all the maps.

Fig.2: HR-XRD patterns for the (0004) reflection as function of the ion fluences (in Xe/cm^2). Patterns are arbitrarily vertically shifted for a better visibility.

Fig.3: Reciprocal space maps of the $(10\bar{1}4)$ reflection (a and b) and the $(1\bar{2}14)$ reflection (c and d), as function of the ions fluence (92MeV $^{129}Xe^{23+}$).

Fig.4: (a) Cross-section TEM micrograph of GaN after irradiation with 92 MeV Xe at 2.10^{14} ions/cm² (with diffraction vector $01\bar{1}0$). The white arrow shows the penetration direction of the ions in the material. HDZ defines the Highly Disordered Zone; (b) the evolution profile of the electron beam intensity detected as a function of the depth, according to the dashed box on the micrograph. The damaged thickness determined from the profile is reported on the TEM picture.

Fig.5: Evolution of hydrostatic and biaxial stresses in the GaN film, as function 92 MeV $^{129}Xe^{23+}$ fluence.

Fig.6: Loading curves by nanoindentation of GaN non-irradiated and irradiated with 92 MeV $^{129}Xe^{23+}$ at 2.10^{13} ions/cm² and 2.10^{14} ions/cm².

Fig.7: Evolution of (a) the elastic modulus and (b) the hardness of pristine and irradiated GaN as a function of the depth, for the different fluences considered.

Fig.8: TEM image underneath indented spots (with a close-up view in the heavily deformed region of GaN thin film) of (a) a non-irradiated GaN film, (b) a GaN film irradiated at a fluence of 2.10^{13} ions/cm².

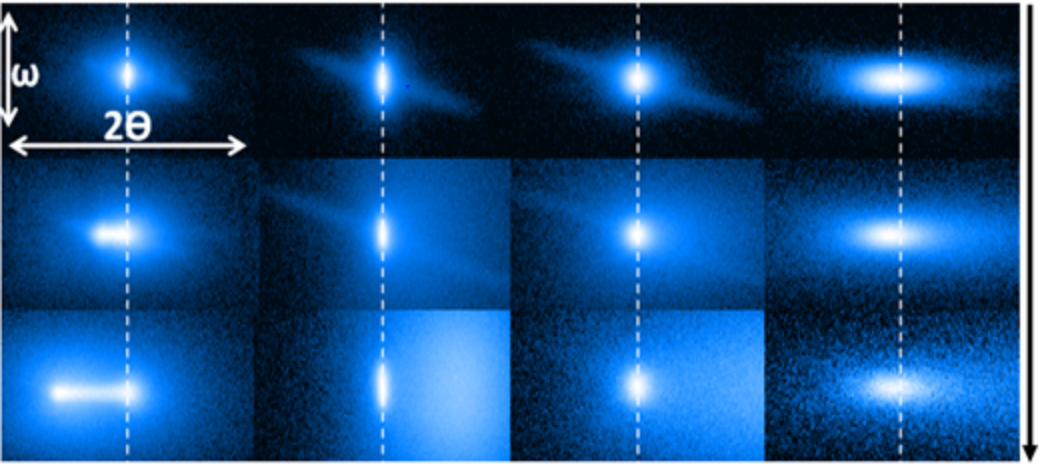
0004
10$\bar{1}$1
11$\bar{2}$2
21$\bar{3}$3
ω
2θ
Virgin
2x10^{13}
2x10^{14}

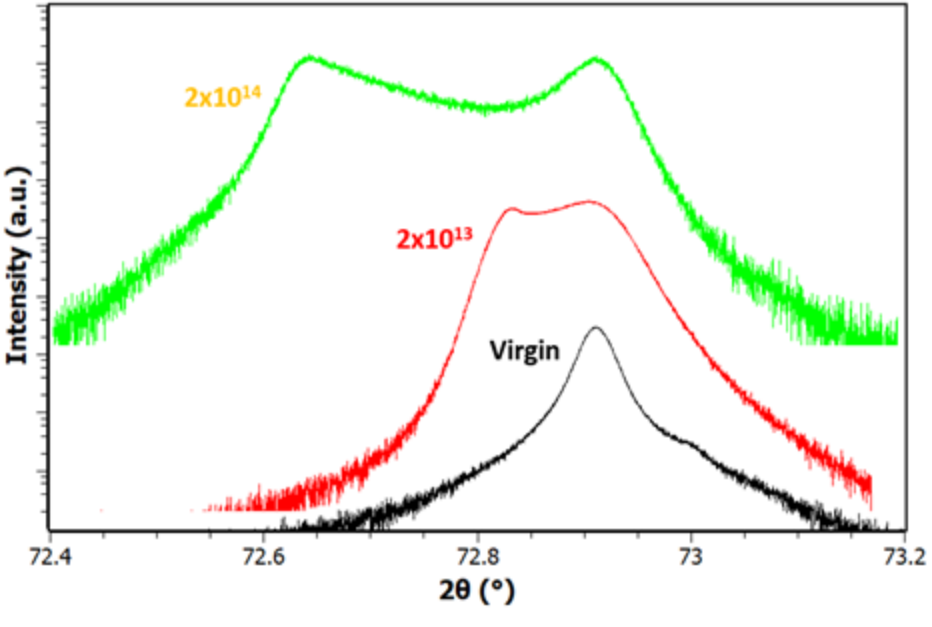
2x10^14
2x10^13
Virgin
Intensity (a.u.)
72.4
72.6
72.8
73
73.2
2θ (°)

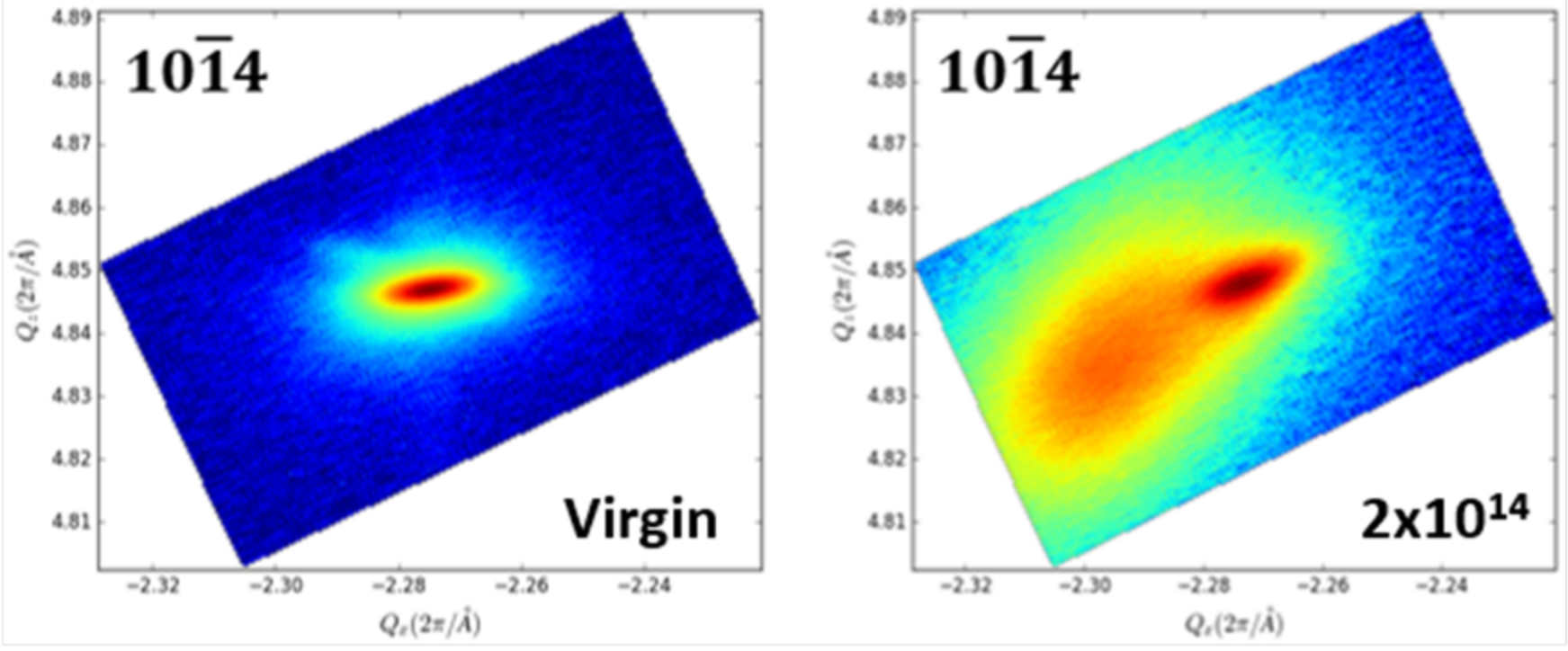
$10\bar{1}4$
Virgin
$10\bar{1}4$
$2x10^{14}$
$Q_z(2\pi/\AA)$
$Q_x(2\pi/\AA)$

(a) (b)

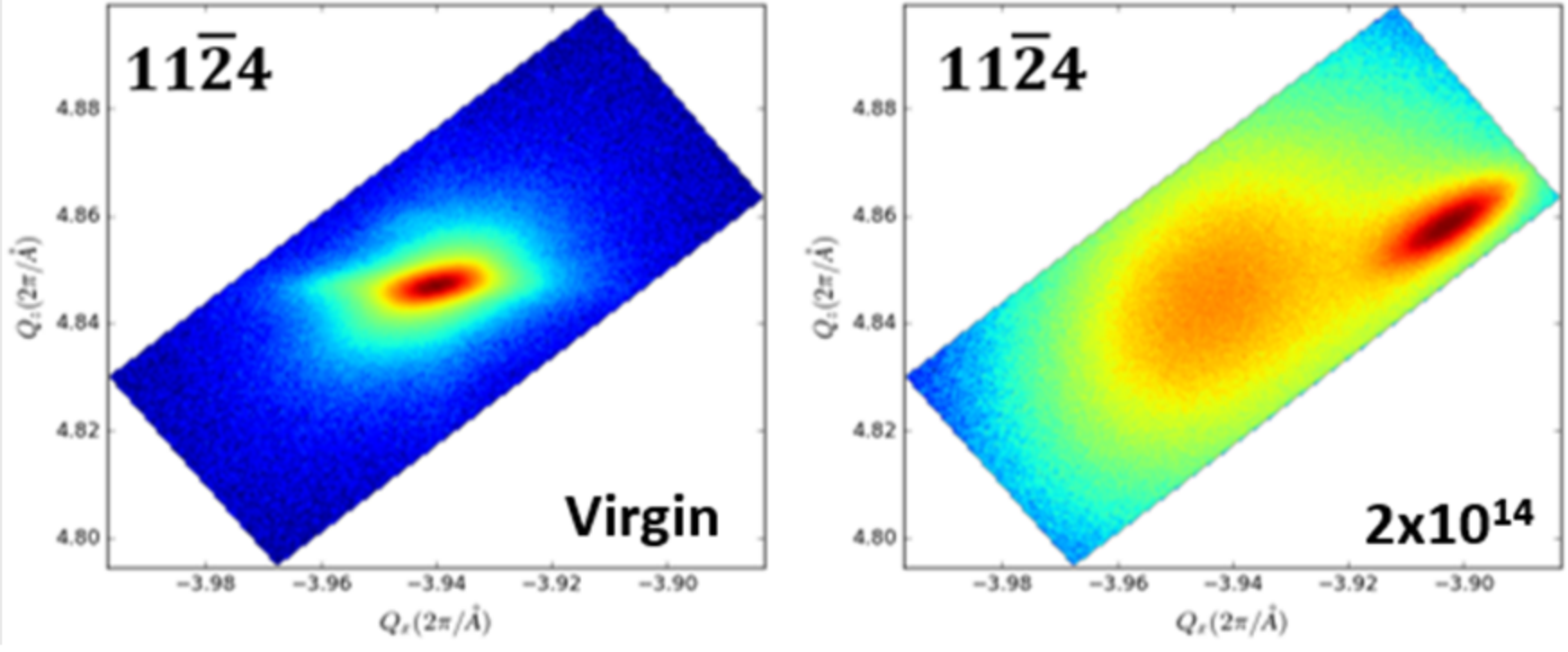
$11\bar{2}4$
Virgin
$11\bar{2}4$
$2x10^{14}$
$Q_z(2\pi/\AA)$
$Q_x(2\pi/\AA)$

(c) (d)

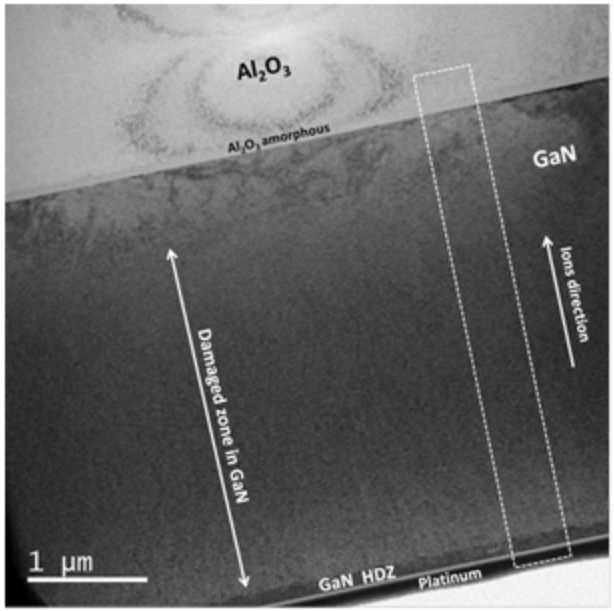
Al_2O_3
Al_2O_3 amorphous
GaN
Damaged zone in GaN
Ions direction
1 µm
GaN HDZ
Platinum

(a)

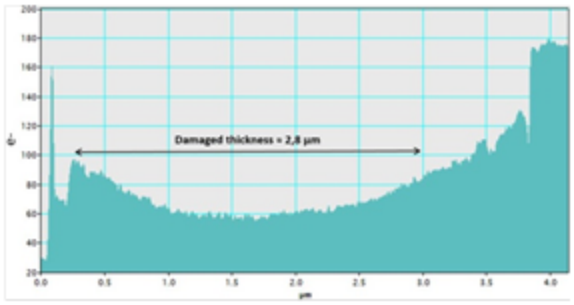
Damaged thickness = 2,8 µm
200
180
160
140
120
100
80
60
40
20
0.0
0.5
1.0
1.5
2.0
2.5
3.0
3.5
4.0
µm

(b)

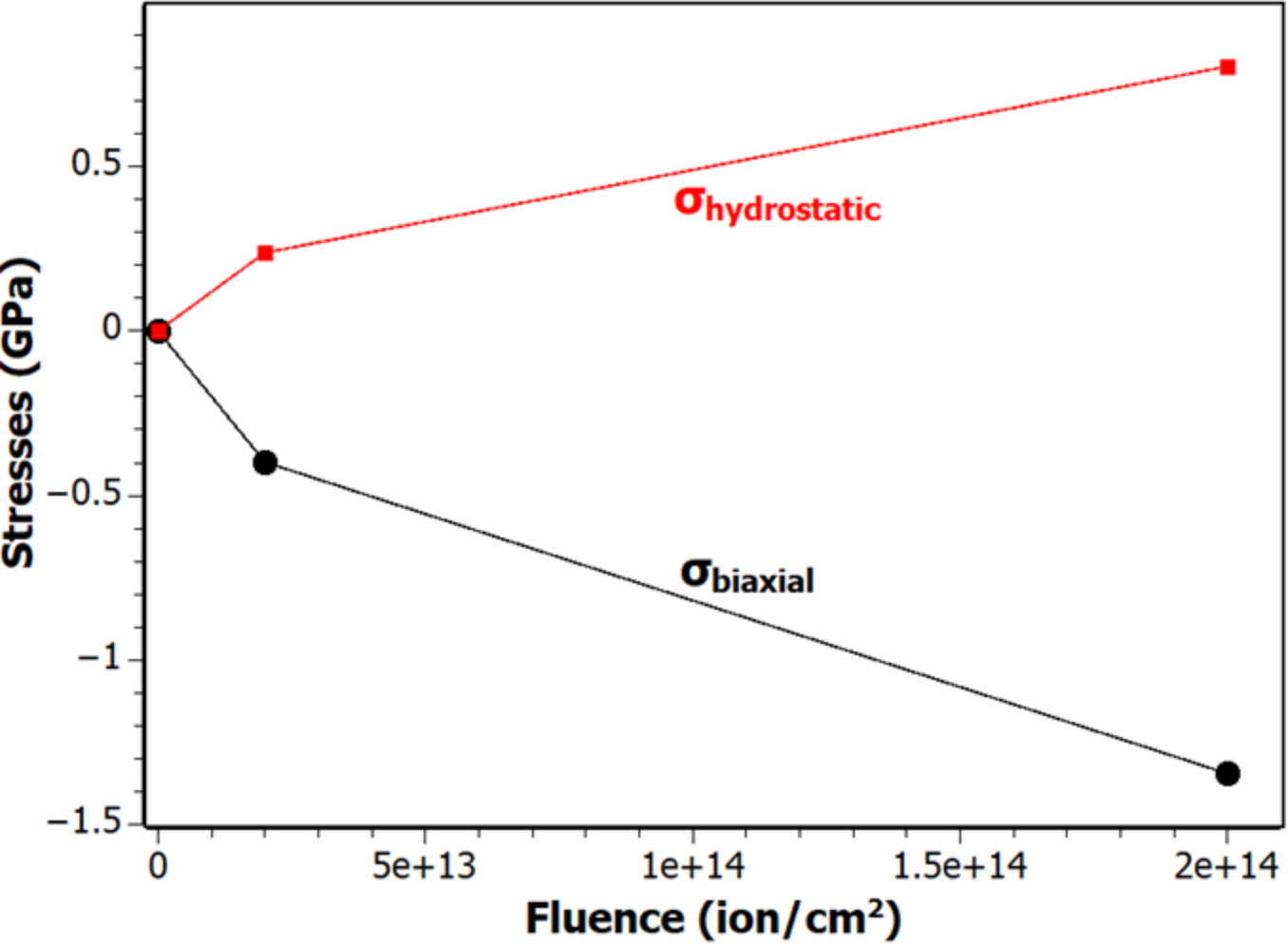
0.5
0
−0.5
−1
−1.5
Stresses (GPa)
σhydrostatic
σbiaxial
0
5e+13
1e+14
1.5e+14
2e+14
Fluence (ion/cm²)

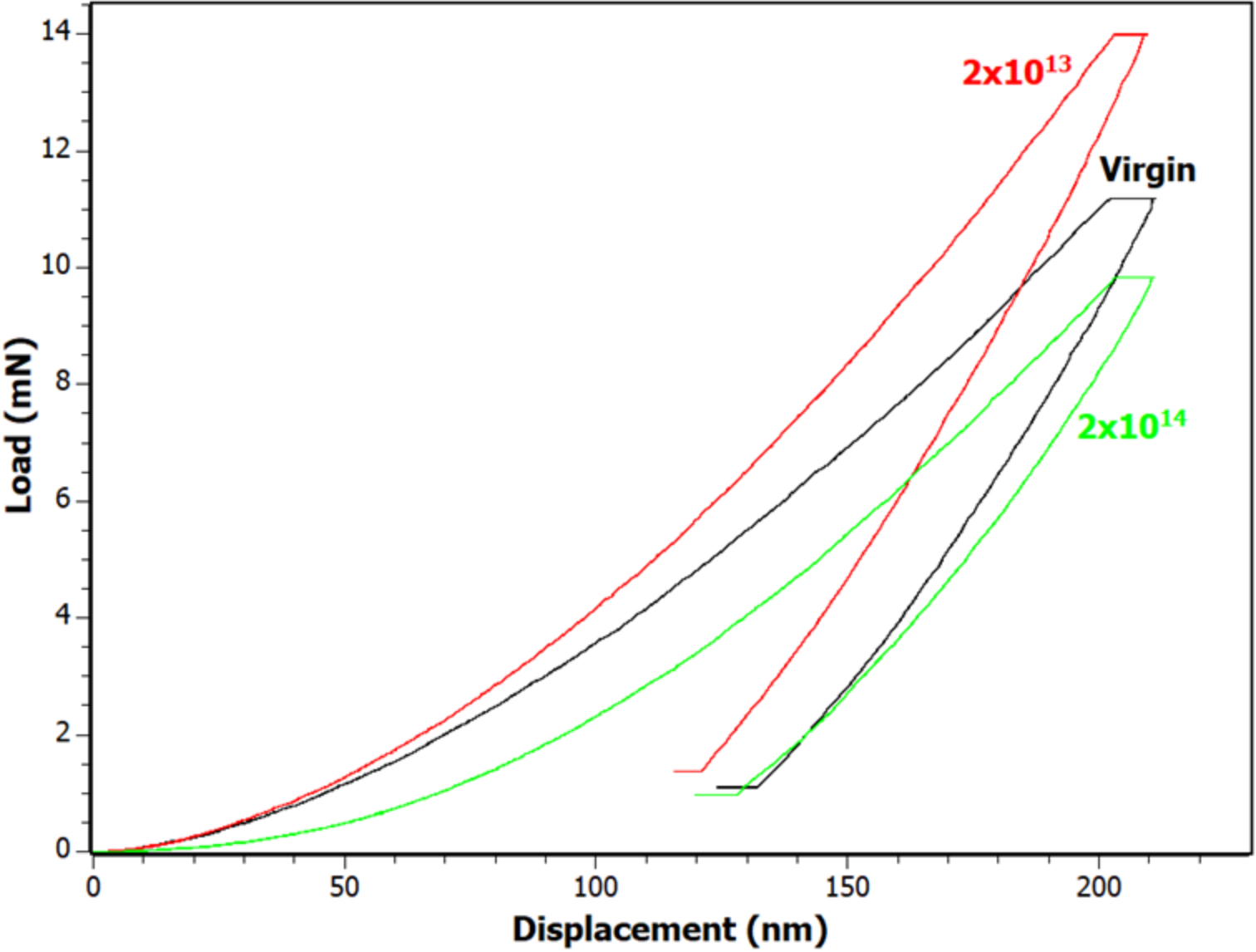
2x10^13
Virgin
2x10^14
Load (mN)
Displacement (nm)
0
2
4
6
8
10
12
14
0
50
100
150
200

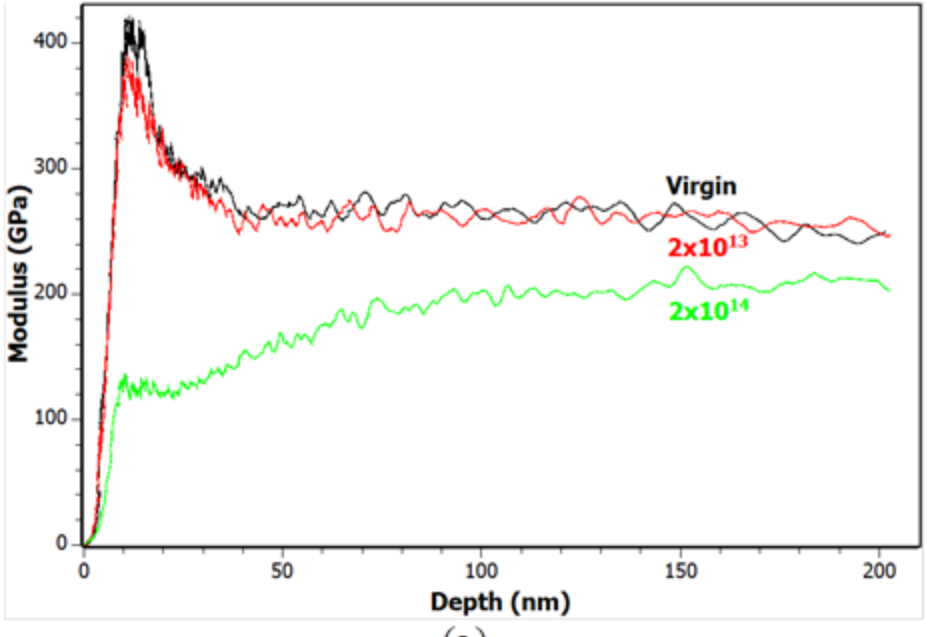
Modulus (GPa)
Depth (nm)
Virgin
2x10^13
2x10^14
0
100
200
300
400
0
50
100
150
200

(a)

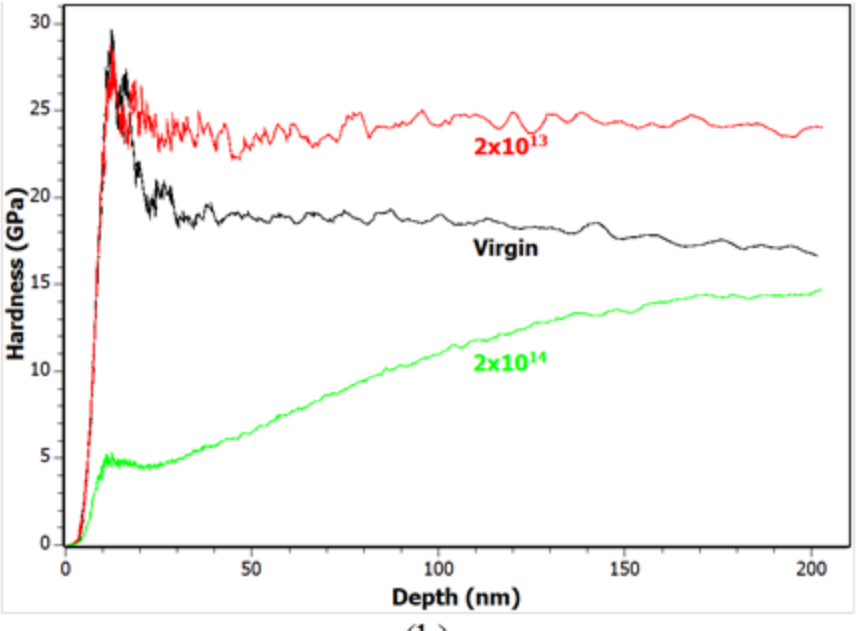
Hardness (GPa)
Depth (nm)
2x10^13
Virgin
2x10^14
0
5
10
15
20
25
30
0
50
100
150
200

(b)

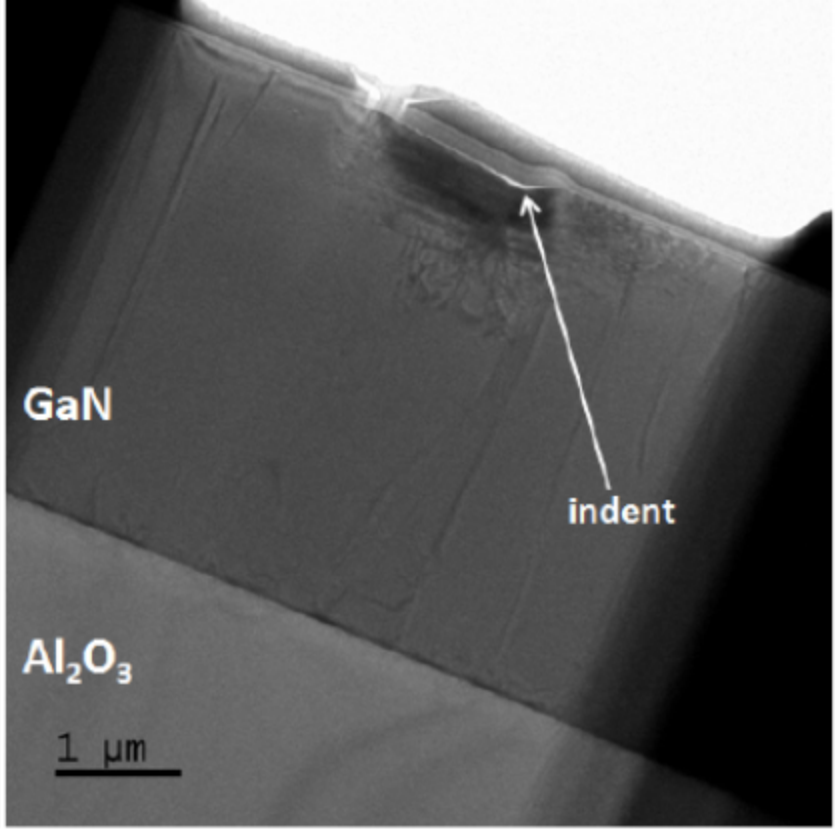
GaN
indent
Al_2O_3
1 μm

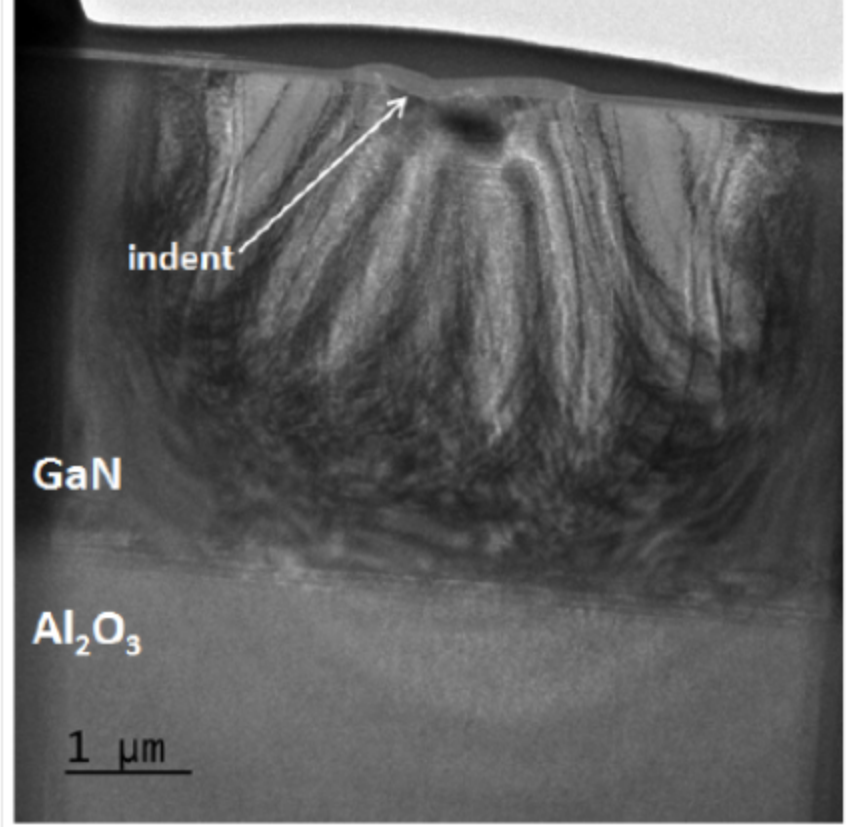
indent
GaN
Al_2O_3
1 μm

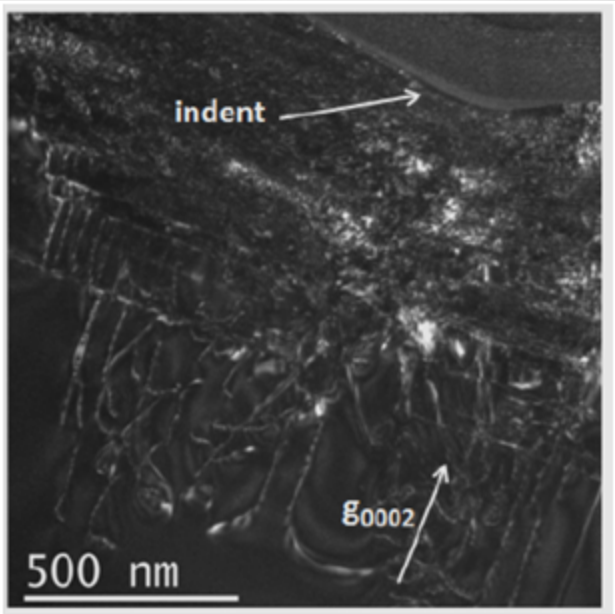
indent
g_{0002}
500 nm

(a)

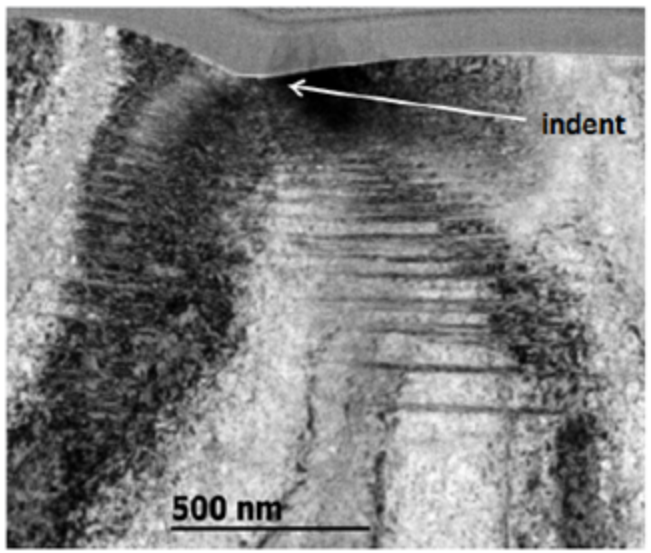
indent
500 nm

(b)